

# Yolk-like Micro/Nanoparticles with Superparamagnetic Iron Oxide Cores and Hierarchical Nickel Silicate Shells

Qunling Fang, Shouhu Xuan,\* Wanquan Jiang, and Xinglong Gong\*

Yolk-like nano/microparticles with superparamagnetic iron oxide (SPIO) cores and hierarchical nickel silicate (NS) shells, designated yolk SPIO@NS, are fabricated by combining the versatile sol-gel process and the hydrothermal reaction, involving the coating of SPIO particles with SiO<sub>2</sub> and transformation of the SiO<sub>2</sub> shells into NS hollow spheres with hierarchical nanostructures. Various yolk/shell nanostructures with tunable NS shell thicknesses and SPIO core sizes are successfully prepared by controlling the experimental parameters. Au nanoparticles can be impregnated into the yolk-like microspheres in situ to form SPIO@NS/Au composite particles and the as-prepared magnetic nanocatalysts show good catalytic activity, using the catalytic reduction of RhB as a model reaction. This facile method can be extended to the synthesis of other encapsulated particles with yolk-like nanostructure.

## 1. Introduction

As a class of nanostructured materials, hollow spheres functionalized with movable cores, known as yolk-like colloidal particles, have attracted growing research efforts because of their unique properties, such as low density, large surface area, multi-functionality and excellent loading capacity.<sup>[1–7]</sup> Over recent decades, several groups have focused on this project and a series of yolk-like nanostructures has been developed, such as Au@Polymer, Au@Carbon, Au@SiO<sub>2</sub>, SiO<sub>2</sub>@TiO<sub>2</sub>, etc.<sup>[8–12]</sup> The outer shells prevent the aggregation of functional cores and provide a useful space for the functional particles in practical applications. Most products have been prepared by templating methods and the design and construction of yolk particles of defined shape, size, composition and function has been technologically achieved.<sup>[13]</sup>

Prof. S. H. Xuan, Prof. X. L. Gong  
CAS Key Laboratory of Mechanical Behavior and Design of Materials  
Department of Modern Mechanics  
The University of Science and Technology of China  
Hefei, 230026, P. R. China  
E-mail: xuansh@ustc.edu.cn; gongxl@ustc.edu.cn

Q. L. Fang  
Center of Novel Functional Molecules  
Department of Chemistry  
The Chinese University of Hong Kong  
Shatin, NT, Hong Kong SAR, P. R. China

Q. L. Fang, Dr. W. Q. Jiang  
Department of Chemistry  
The University of Science and Technology of China  
Hefei, 230026, P. R. China

DOI: 10.1002/adfm.201002191

Yolk-like particles with magnetically responsive cores and functional shells have gained much attention due to their unique feature of separability, which makes it possible to use such particles to realize magnetic targeting drug delivery, recycling of nanocatalyst, selective capture of target objects and magnetically controllable on-off reactions.<sup>[14–17]</sup> Zhao et al. reported rattle-type magnetic mesoporous spheres using Fe<sub>2</sub>O<sub>3</sub> as the precursor template, and this product could realize a significantly higher storage capacity of drug compared to those without the hollow cavity.<sup>[18]</sup> To enlarge the size of the hollow cavity, carbon spheres with iron precursor were employed to synthesize yolk-like Fe<sub>3</sub>O<sub>4</sub>@SiO<sub>2</sub> mesoporous spheres with

tunable size and shell thickness, which exhibited high drug loading capacity and bio-compatibility.<sup>[19]</sup> Besides the spherical shape, non-spherical yolk-like particles, such as Fe<sub>3</sub>O<sub>4</sub>@Carbon ellipsoids, Fe<sub>3</sub>O<sub>4</sub>@SiO<sub>2</sub> nanorods and double-walled SnO<sub>2</sub> nano-cocoons with movable magnetic cores, have also been successfully achieved.<sup>[20–23]</sup> However, to date, all the reported synthetic procedures are rather complex and the products are ferromagnetic. Superparamagnetic materials do not retain any magnetization in the absence of an externally applied magnetic field, while the ferromagnetic products form aggregations due to remanence.<sup>[24–31]</sup> Therefore, yolk-like particles with superparamagnetic inner cores are of great interest for application in magnetic resonance imaging, hyperthermia, separation and purification of biomolecules, drug delivery and catalysis.<sup>[32]</sup>

Hierarchical nanoarchitectures assembled from nanoscale units have stimulated tremendous interest since they can avoid aggregation while maintaining high specific surface areas.<sup>[33–37]</sup> The combination of a hierarchical nanoarchitecture with superparamagnetic character to form yolk-like particle represents a promising type of nanomaterial, and the special multifunctional nanostructure makes a product possible that has low density, high specific surface areas, void properties, magnetic targeting and so on. However, reports on preparation of yolk-like particles with hierarchical shells and superparamagnetic cores are relatively scarce, partly because of the difficulty in coating the magnetic core with a uniform hierarchical shell. In order to improve their performance in practical applications,<sup>[13,38]</sup> precise structure and size control of both hierarchical shells and functional cores via a facile and efficient way is desirable to fully exploit these tiny vesicles. Magnetic separation provides a very convenient approach for removing and recycling magnetic composite particles by applying an appropriate magnetic

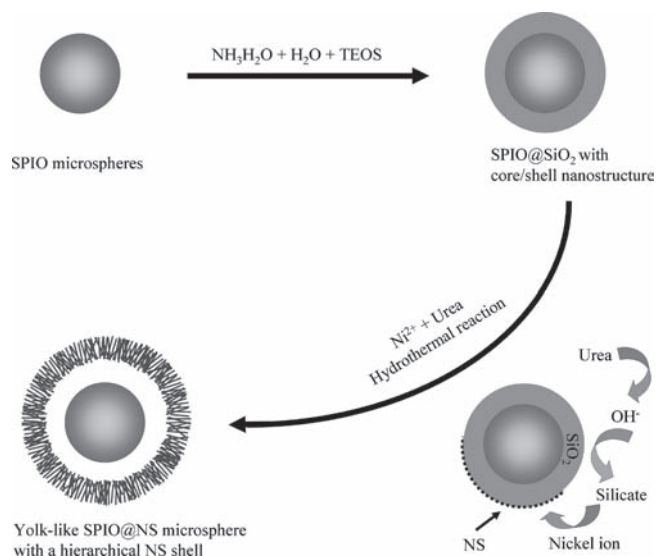
field, which enables wide use in nanocatalysis.<sup>[39–42]</sup> However, most efforts have been devoted to immobilizing nanocatalysts on the surface of magnetic spheres or impregnating them into the pores of the magnetic mesoporous materials;<sup>[39,41,43]</sup> little work has succeeded in designing yolk-like magnetic particles as carriers for nanocatalysis. In recent years, there has been an increasing interest in the utilization of silicate nanomaterials in adsorption, separation and catalytic applications.<sup>[35,44,45]</sup> Compared to polymer and silica materials that have been studied, silicate has exhibited much higher stability in various chemical and physical environments, such as acidic or basic media, organic solvents and at high temperatures and pressures. In considering their high specific surface area, high porosity, surface activity and hierarchical nanostructure, the combination of the hierarchical silicate with superparamagnetic nanomaterials together to form yolk-like nanostructure, which can be used in catalyst immobilization, is highly desirable.

Here, we report a simple method to construct yolk-like particles with hierarchical nickel silicate (NS) shells and movable superparamagnetic iron oxide (SPIO) cores. The yolk-like SPIO@NS particles were formed through a hydrothermal route based on a SPIO@SiO<sub>2</sub> sacrificial templating process. Various yolk/shell structures with different shell thicknesses and core sizes have been successfully prepared by controlling the experimental parameters. The product is demonstrated to be a good carrier for Au nanocatalyst by using catalytic reduction of RhB as a model reaction. To the best of our knowledge, this is the first report on the synthesis of yolk-like SPIO@NS particles for noble nanocatalyst immobilization. A formation mechanism is proposed and the synthetic parameters are discussed.

## 2. Results and Discussion

Yolk-like particles are usually prepared based on a template-assisted approach, in which the core particle is coated with double shells of different materials and then the inner shell is selectively removed. However, these methods need the preparation of three layered core/shell nanostructures, and the synthetic procedures are multi-step and complex.<sup>[2,9,11,12,18,19]</sup> Here, unique yolk-like SPIO@NS microspheres with superparamagnetic cores and hierarchical shells are fabricated through a two-step method. **Scheme 1** illustrates the synthetic procedure. Step 1 involves the uniform coating of SPIO microsphere with a layer of SiO<sub>2</sub> to produce SPIO@SiO<sub>2</sub> core/shell particles. This silica coating step by a modified Stöber's process is highly reproducible<sup>[46,47]</sup> and the silica coating acts as not only the template but also the starting material for the yolk shell. In the second hydrothermal step, the SiO<sub>2</sub> is dissolved to form silicate anions under the alkaline condition and react with the Ni<sup>2+</sup> cations to give the hierarchical NS nanostructures. Finally, yolk-like SPIO@NS microspheres are achieved.

The morphology of the obtained particles is first characterized using scanning electron microscopy (SEM). It is found that the products are composed of sphere-like particles and the size is around 500 nm, as shown in **Figure 1a**. A closer look (the inset of **Figure 1a**) shows that these microspheres are hierarchical and the surface is assembled by a large number of nanosheets. To further investigate their nanostructure,



**Scheme 1.** Graphical representation of the fabrication of yolk-like SPIO@NS microspheres with superparamagnetic cores and hierarchical shells.

transmission electron microscopy (TEM) is employed. **Figure 1b** shows a low magnification TEM image, which clearly indicates that the as-prepared microspheres exhibit a typical yolk-like nanostructure. As can be seen from the image, most NS yolk shells encapsulate only one SPIO microsphere, which is usually not located in the center of the hollow spheres. The encapsulated SPIO sphere is free to move within each hollow particle, at least when filled with liquid.<sup>[13]</sup> From a higher magnification TEM image (**Figure 1c**), it is very clear that the yolk-like particles are well dispersed on the copper grid, which indicates the uniform nature of our product. The average size of the particles is

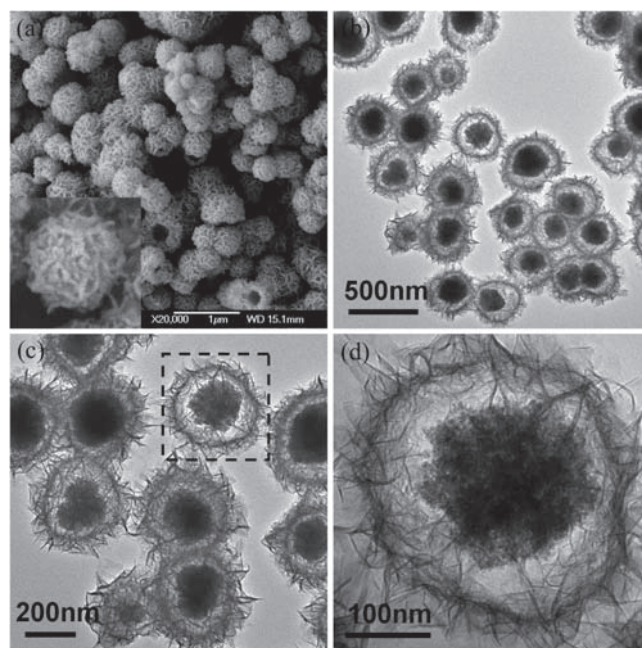


**Figure 1.** SEM (a) and TEM images (b,c,d) of the yolk-like SPIO@NS microspheres with superparamagnetic cores and hierarchical shells.

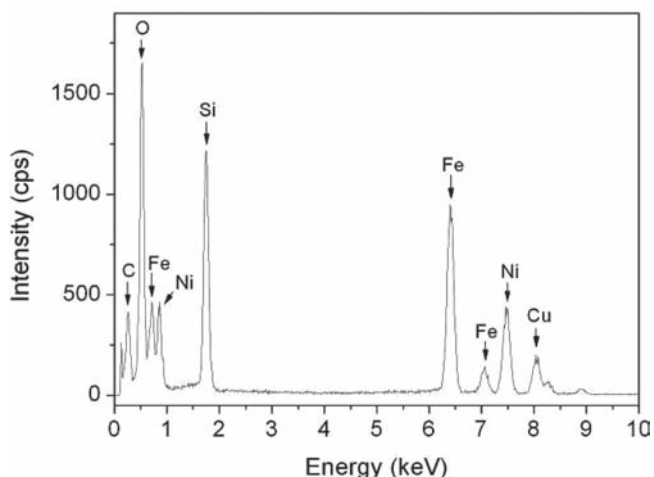


**Figure 2.** EDS spectra of the yolk-like SPIO@NS microspheres with superparamagnetic cores and hierarchical shells.

approximately 400 nm and the shell thickness is about 60 nm. Figure 1d shows the TEM image of a single SPIO@NS microsphere with yolk-like nanostructure. A detailed look shows that the yolk shell is hierarchical and the shell is assembled by a large number of nanosheets, which agrees well with the SEM observation. Moreover, the central particle is nearly spherical with a size about 200 nm, which is composed of small primary nanocrystals with a size of 5–7 nm.

Energy-dispersive spectroscopy (EDS) analysis of the yolk nanostructure indicates the presence of Fe, Ni, Si, and O, proving the presence of iron oxide and nickel silicate (**Figure 2**). The signals of Cu and C in the EDS spectrum originate from the carbon-coated copper grid. The crystallographic structure of the product is further determined by XRD. **Figure 3a** shows the XRD pattern of the SPIO precursor, which can be indexed to be face-centered cubic magnetite (JCPDS Card No. 19-629). The broad nature of the patterns clearly indicates the SPIO microsphere is composed of small nanocrystals, which agrees well

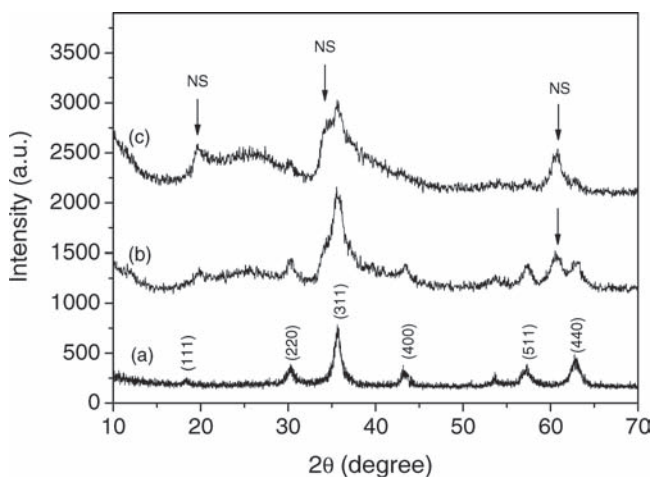


**Figure 3.** XRD patterns of the SPIO microspheres (a), yolk-like SPIO@NS microparticles (b), and yolk-like SPIO@NS microparticles with thick NS shells (c).

with the TEM analysis. Here, a small proportion of maghemite may be existed in the microspheres due to the magnetite nanocrystals are very easily oxidized to be maghemite.<sup>[42]</sup> As shown in Figure 3b, the representative XRD pattern of the as-synthesized yolk-like nanostructure indicates that both SPIO and NS existed. However, due to the low concentration of NS, only two low intensity peaks located at 20° and 61° can be clearly observed. The NS is indexed to be nickel silicate hydroxide hexagonal phase (JCPDS No. 43-0664) and such substance is defined as NS in this work. The apparent broadening of their peaks indicates the NS shell is composed of nanoscaled crystals with low crystallinity.<sup>[33]</sup> Based on the combined XRD, TEM, and EDS results, yolk-like particles with iron oxide cores and hierarchical NS shells have been successfully fabricated by using such a simple method.

The synthetic process of the yolk-like product is monitored by TEM image to investigate the formation mechanism. Figure S11a and b (see the Supporting Information) show TEM images of the uniform SPIO microspheres with typical cluster-like nanostructure (200 nm). The sizes of these SPIO particles are tunable from 10 to 200 nm,<sup>[46]</sup> hence they are the most suitable templates for the synthesis of yolk-like products with controllable core sizes. Indeed, the superparamagnetic nature of the SPIO particle is critical in our method, since the ferromagnetic property often led to the formation of large SPIO aggregation during the final NS coating process. The silica coating is conducted by a versatile sol-gel process and the shell thicknesses can be controlled by varying the SPIO and TEOS concentrations. In this work, the yolk-like product cannot be achieved by using SPIO@SiO<sub>2</sub> with thin SiO<sub>2</sub> shell as the template. As shown in Figure S11c and d (see the Supporting Information), uniform SPIO@SiO<sub>2</sub> microspheres with 50 nm shell thickness are employed to synthesize the final yolk-like product. Through a sacrificial templating hydrothermal process, yolk-like particles with iron oxide cores and hierarchical NS shells were obtained (Figure S11e). A closer look (Figure S11f) shows that the inter-diameter of the NS shell is consistent with the diameter of the SPIO@SiO<sub>2</sub> core/shell microsphere, which clearly proves that the SiO<sub>2</sub> shell actually acted as a reactive sacrificial template for the formation of the hierarchical NS shells.

Time-dependent TEM observation of the hydrothermal process is also conducted to understand how the yolk-like nanostructures are generated. At the beginning of the reaction, an uniform alkaline solution was formed due to the thermal decomposition of the urea under hydrothermal conditions, which would lead to the dissolution of the SiO<sub>2</sub> shell as soon as possible.<sup>[48]</sup> In this case, the silicate anions would react with the Ni<sup>2+</sup> cations to give NS nanograins. The as-formed NS nanograins that generated nearby the SiO<sub>2</sub> (the concentration of the silicate anions nearby the SiO<sub>2</sub> is relatively higher than the other places in the autoclave) were preferentially deposited on the surface of the SiO<sub>2</sub> shell (Scheme 1). **Figure 4a** shows the TEM image of the product after the hydrothermal reaction was conducted for 0.5 h. In comparison to the pristine SPIO@SiO<sub>2</sub> (Figure S11d in the Supporting Information), the surface of the as-prepared microsphere is rather rough, which clearly indicates the in situ dissolution of the SiO<sub>2</sub> and formation of the NS. With increasing of the reaction time, more nanograins are deposited to form an integrated NS shell and the SiO<sub>2</sub> are

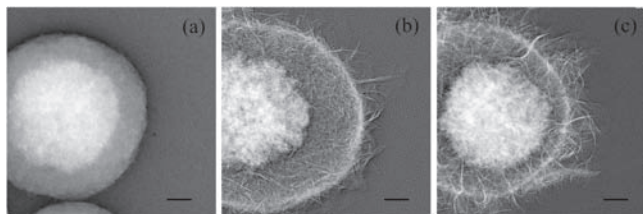


**Figure 4.** TEM images of products synthesized under different hydrothermal time: 0.5 h (a), 6 h (b) and 18 h (c); the scale bar is 50 nm.

dissolved to form the hollow interior. When the reaction time was 6 h, a yolk-like SPIO@NS microsphere with a thin NS shell was obtained (Figure 4b). If the reaction time was further prolonged, the growth of the NS shell would be processed continuously, and then a thicker and denser NS shell with hierarchical nanostructure was achieved. Figure 4c shows the TEM image of the yolk-like SPIO@NS microsphere synthesized after 18 h. Compared with Figure 4b, the NS shell is much thicker, which indicates that the longer reaction time can produce more NS materials in the product. When the reaction time is further prolonged to 36 h, yolk-like SPIO@NS microsphere with 60 nm shell thickness (Figure 1) are successfully synthesized by using a hydrothermal route based on a SPIO@SiO<sub>2</sub> sacrificial templating process, whereas the SiO<sub>2</sub> shell actually acted not only as the precursor for the NS material but also as a sacrificial template for the hollow structure.

In this work, the NS shell thicknesses are dependent on the Ni<sup>2+</sup> concentrations used in the hydrothermal reaction. Figure 5a–c shows TEM images of the synthesized yolk-like nanostructures using SPIO@SiO<sub>2</sub> microspheres with 50 nm

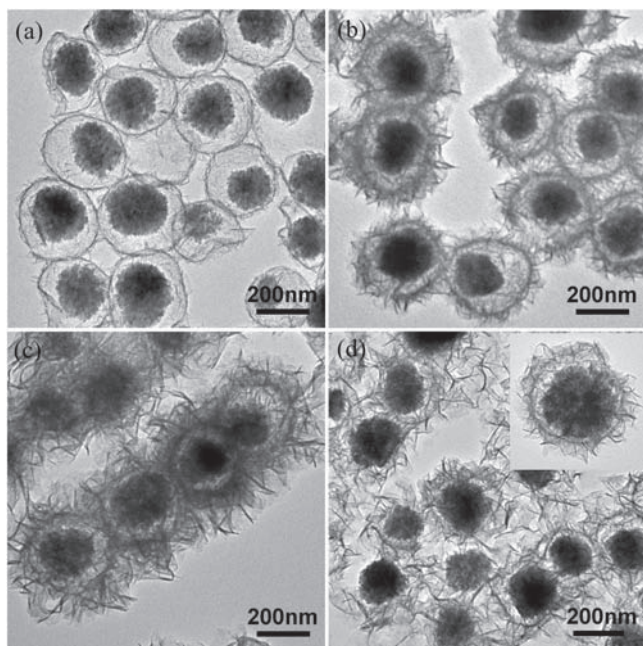


**Figure 5.** TEM images of yolk-like SPIO@NS nanostructure with different shell thicknesses (a,b,c) by using uniform SPIO@SiO<sub>2</sub> microspheres with 50 nm shell thickness as the template; TEM images of yolk-like SPIO@NS nanostructure (d) by using uniform SPIO@SiO<sub>2</sub> microspheres with 25 nm shell thickness as the template.

shell thickness as the templates. Yolk particles using 60% of the standard Ni<sup>2+</sup> concentration (the concentration of Ni<sup>2+</sup> used for the Figure 1 is defined as standard value) as starting material are presented in Figure 5a. The yield of the product is very high, and almost each SPIO particle is encapsulated by a thin NS shell with a thickness of 20 nm. As can be seen from Figure 5b, with increasing of the Ni<sup>2+</sup> concentration (to the standard value), the shell thickness increases to 60 nm. The further increasing of the Ni<sup>2+</sup> concentration (140% of the standard value) leads to the 100 nm shell thickness (Figure 5c). However, in this case, the as-prepared products are not well-dispersed and most of the particles are lightly agglomerated by the coalescence of the outer hierarchical NS shells. Therefore, in order to obtain uniform yolk-like particles, the Ni<sup>2+</sup> concentration should be controlled below the standard value.

It is also noticeable that the uniform yolk-like nanostructure can not be pursued when SPIO@SiO<sub>2</sub> microspheres with 25 nm shell thickness were used (Figure S12, see the Supporting Information), as mentioned above. Figure S13a shows the TEM image of the product synthesized under standard Ni<sup>2+</sup> concentration. Part of the product shows a core/shell nanostructure (Figure S13b and c) and the other parts are naked SPIO microspheres (not shown). The SPIO@NS microspheres with yolk-like nanostructures are only occasionally observed during TEM examination if they do exist, as can be seen from the Figure S13d. Interestingly, in this case, if the Ni<sup>2+</sup> concentration is 140% of the standard value, yolk-like product also can be achieved (Figure 5d). Unfortunately, the hierarchical NS shells are not stable, being destroyed under sonication at low intensity. Therefore, for the fabrication of uniform yolk-like nanostructures, SPIO@SiO<sub>2</sub> microspheres with thick SiO<sub>2</sub> shell thickness are preferred.

Interestingly, when the diameters of the SPIO core particles decreased from 200 to 75 nm, the yolk-like nanostructure also can be produced (Figure 6a–c and Figure S14). Figure 6a shows a typical TEM image of the yolk SPIO@NS nanospheres with 75 nm core size. All these particles are well dispersed on the copper grid and each particle is composed of one hierarchical shell and one cluster-like core (Figure 6b). The average size of the yolk particle is about 200 nm and the shell thickness is about 15 nm (Figure 6c). The inner-size of the yolk nanoparticle is similar to the outer size of the SPIO@SiO<sub>2</sub> precursor (inset of Figure 6a and Figure S15), which further proves that the SiO<sub>2</sub> shell act as both template and precursor for the NS hierarchical shell. By using this simple method, the yolk SPIO@NS microspheres with 200 nm core size and 15 nm shell thickness also can be easily synthesized (Figure 6d). It is likely that the hierarchical NS shell can accommodate SPIO particles with different sizes through adjusting its SiO<sub>2</sub> shell thickness. Due to the high alterability of the SPIO size, SiO<sub>2</sub> coating thickness, and the Ni<sup>2+</sup> concentration, yolk SPIO@NS microspheres with defined core size, interior cavity, and shell thickness can be technically designed. Furthermore, this method can be extended to the synthesis of other encapsulated particles.

The magnetic properties of the yolk SPIO@NS microspheres have been investigated using a vibrating sample magnetometer (VSM). Figure 7a shows the hysteresis loop of typical yolk SPIO@NS microspheres measured by sweeping the external field between –0.6 to 0.6 T at room temperature. No obvious

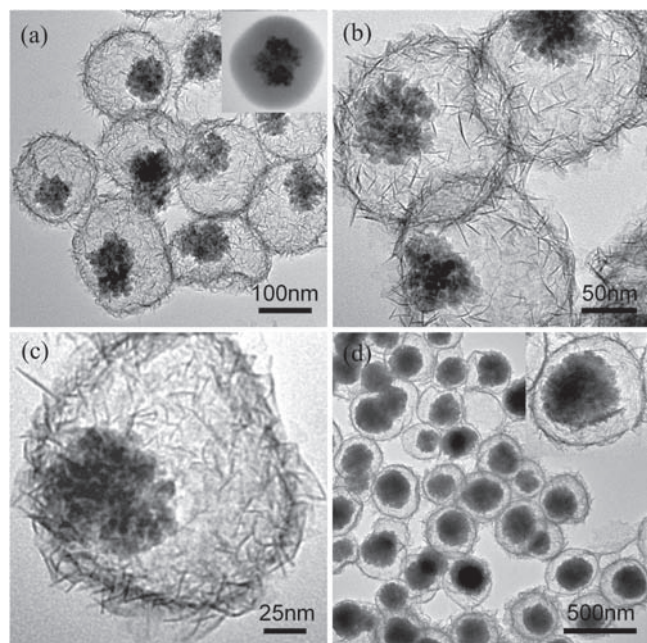


**Figure 6.** TEM images of yolk-like SPIO@NS nanostructure with different core sizes: 75 nm (a,b,c) and 200 nm (d); the inset of (a) is the TEM image of the SPIO@SiO<sub>2</sub> precursor for yolk-like SPIO@NS nanostructure with 75 nm core sizes.

remanence or coercivity is observed in the magnetization curve at room temperature, suggesting a superparamagnetic character.<sup>[24,28,29]</sup> With the superparamagnetic property, capillary blockage by aggregations formed by residual magnetism after removal of the applied field would be avoided. The saturated mass magnetization is estimated to be 12.9 emu g<sup>-1</sup>. Therefore, based on the combined VSM and above TEM, XRD, EDS results, yolk-like particles with hierarchical nickel silicate shell and movable superparamagnetic iron oxide cores, which can be easily separated from the reaction solution by applying a relatively low magnetic field,<sup>[49]</sup> were successfully prepared.

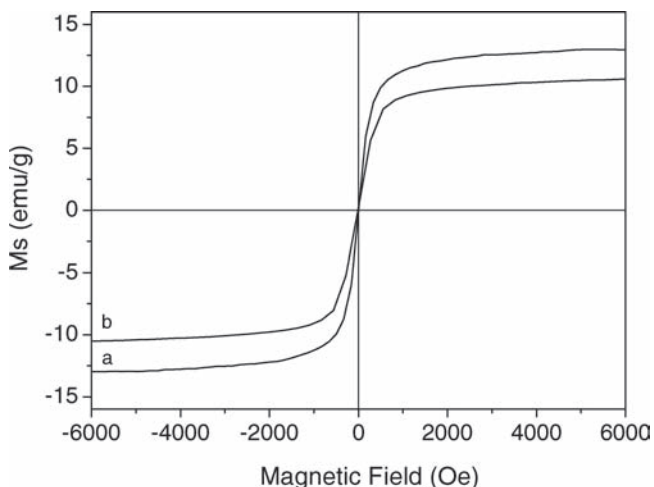


**Figure 7.** Hysteresis loop measurements of yolk-like SPIO@NS microspheres (a) and yolk-like SPIO@NS/Au nanocomposites (b) at room temperature.

The BET (Brunauer-Emmett-Teller) surface areas analysis shows that the surface area of the as-prepared yolk-like SPIO@NS microspheres (Figure 1) is 89.6 m<sup>2</sup>g<sup>-1</sup>. The yolk particles have a relatively large specific surface area, which is mainly caused by the existence of mesopores embedded in the yolk spheres.<sup>[44]</sup> Therefore, it would be applied as a supporter in catalytic area. Here, Au nanoparticles with controllable weight ratio were immobilized into the above yolk-like SPIO@NS microspheres (the yolk-like spheres (Figure 1) were functionalized by APTES to give amine groups onto the surfaces of the hierarchical nanounits before the Au immobilization) by impregnating particles in a HAuCl<sub>4</sub> aqueous solution, followed by a simple NaBH<sub>4</sub> reducing process. **Figure 8a** shows a low magnification TEM image of as-prepared SPIO@NS/Au nanocomposites, which indicates that the products keep the yolk-like nanostructure very well. From the TEM image with a higher resolution (Figure 8b), clearly, the spherical SPIO microsphere is well encapsulated in a hierarchical yolk shell. Furthermore, there are many black dots decorated into the yolk-like nanostructure, which can be indexed to be Au nanoparticles. Figure 8c shows a representative TEM image of a single SPIO@NS/Au composite microsphere. It is clear that all the Au nanoparticles are homogeneously located on or within the hierarchical NS shell. No individual nanoparticles are found in the solution, indicating the well combination between the Au nanoparticle and the yolk-like carrier. Most Au nanoparticles are uniform in size and well-dispersed in the hierarchical shell without excessive aggregation. The composition of the SPIO@NS/Au composite was investigated by XRD (**Figure 9**). In comparison to the XRD pattern of the yolk-like SPIO@NS microspheres (Figure 3b), three additional peaks at 38°, 43° and 65°, which represent the Bragg reflections from (111), (200), and (220) planes of Au, are observed, showing the existence of Au nanoparticles in the SPIO@NS/Au composite. The EDS result in Figure 8d shows that the elemental compositions of the nanocomposites are Fe, Si, Ni, O and Au, proving the presence of iron oxide, nickel silicate and Au, agrees well with the XRD analysis. All the above results indicate that Au nanoparticles can be well carried by the yolk particle to form SPIO@NS/Au composite with defined yolk-like nanostructure.

The loading efficiency of the Au nanoparticles in the yolk SPIO@NS particles were tuned by simply altering the concentration of HAuCl<sub>4</sub>. Interestingly, by changing the HAuCl<sub>4</sub> concentration, yolk SPIO@NS particles loaded with different kinds of Au nanoparticles can be obtained. **Figure 10a** shows a TEM image of the SPIO@NS/Au composite prepared with 1.56 × 10<sup>-4</sup> MHAuCl<sub>4</sub> (defined as SPIO@NS/Au(1)). In this case, the size of the synthesized Au nanoparticle is about 4 nm and all the Au nanoparticles are located within the hierarchical NS shell (Figure SI6a). Surprisingly, when the HAuCl<sub>4</sub> concentration increases to 3.13 × 10<sup>-4</sup> M, besides 4 nm Au nanoparticles located within the NS shells, a large and irregular Au particle was formed (Figure 10b). After carefully investigation, it is found that the irregular Au particle is located inside the hollow NS shell (Figure SI6b). Moreover, only one large Au particle located in one yolk-like microsphere, which indicate the as-prepared yolk SPIO@NS/Au composite (defined as SPIO@NS/Au(2)) can be used as the Au reservoir. With further increasing of the HAuCl<sub>4</sub> concentration to 6.25 × 10<sup>-4</sup> M, the size of the Au

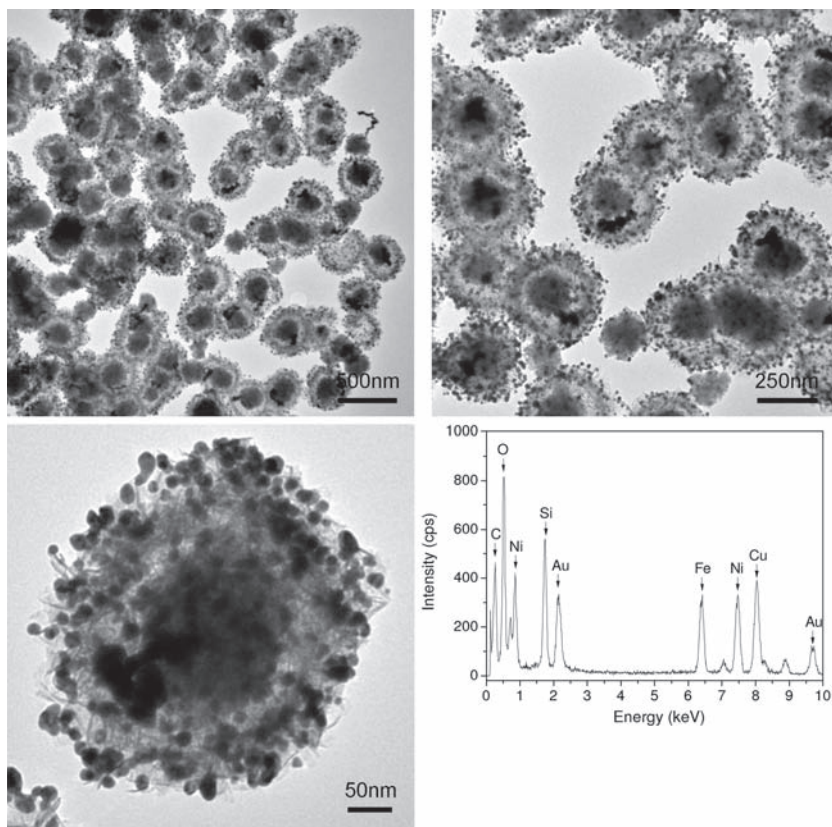


**Figure 8.** TEM images (a,b,c) and EDS (d) spectra of the as-prepared SPIO@NS/Au nanocomposite.

nanoparticles located within the NS shell increases to 12 nm (Figure 10c). In addition, as can be seen from the TEM image (Figure S16c), an irregular and large Au nanoparticle is also encapsulated within the hollow interior (defined as SPIO@NS/Au(3)). At last, when the  $\text{HAuCl}_4$  concentration reaches  $1.25 \times 10^{-3} \text{ M}$ , a large number of Au nanoparticles of 12 nm are located within the hierarchical NS shell (Figure 10d and Figure S16d).

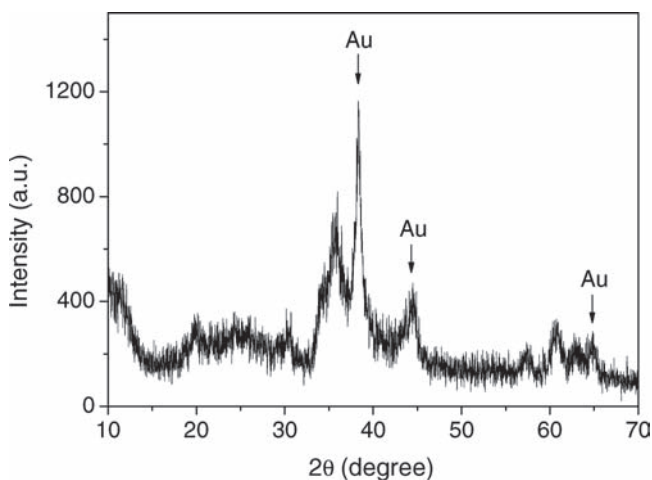


**Figure 9.** XRD pattern of the yolk-like SPIO@NS/Au composite nanoparticles.

In comparison to the SPIO@NS/Au composite prepared with  $6.25 \times 10^{-4} \text{ MHAuCl}_4$ , the Au loading ratio increases sharply. The weight ratio of the Au nanoparticles in the SPIO@NS/Au composite is about 30% w/w (defined as SPIO@NS/Au(4)), which is much higher than the previous report.<sup>[50]</sup> Figure S17 shows the UV-vis absorption spectrums of the as-prepared SPIO@NS/Au composite. As shown in Figure S17a, original yolk particles display one peak at 420 nm, which can be attributed to the absorption of SPIO cores. If only 4 nm Au nanoparticles were located onto yolk particles, no obvious peaks for Au were observed (SPIO@NS/Au(1) and SPIO@NS/Au(2)) due to the low loading ratio. When the weight ratio of the Au nanoparticles increased, a peak centered at 532 nm was obtained (SPIO@NS/Au(3)). If the Au ratio becomes higher (SPIO@NS/Au(4)), the peak shift to 552 nm and the intensity increased sharply. Obviously, the plasmon band can be controlled by varying the loading ratio of the Au nanoparticles, which enable these yolk SPIO@NS/Au nanocomposites be applied in SERS.<sup>[51–54]</sup>

The catalytic performance of SPIO@NS/Au(3) was explored in the reduction of RhB dye, which was conducted in the presence of  $\text{NaBH}_4$  as a model system.<sup>[41,50]</sup> Figure 11 shows the UV-vis spectra for the reduction of RhB measured at a different times during the

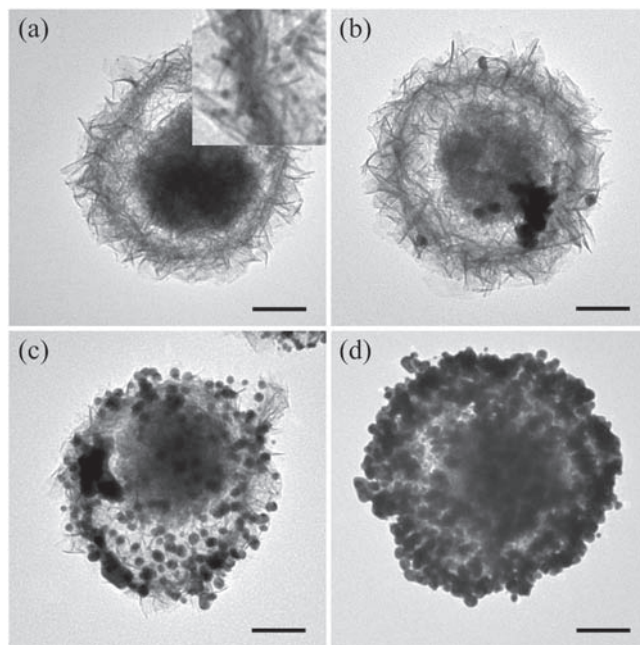


**Figure 10.** TEM images of the as-prepared SPIO@NS/Au nanocomposites with different Au loading concentration:  $1.56 \times 10^{-4} \text{ M}$  (a),  $3.13 \times 10^{-4} \text{ M}$  (b),  $6.25 \times 10^{-4} \text{ M}$  (c), and  $1.25 \times 10^{-3} \text{ M}$  (d). The scale bar represents 100 nm.

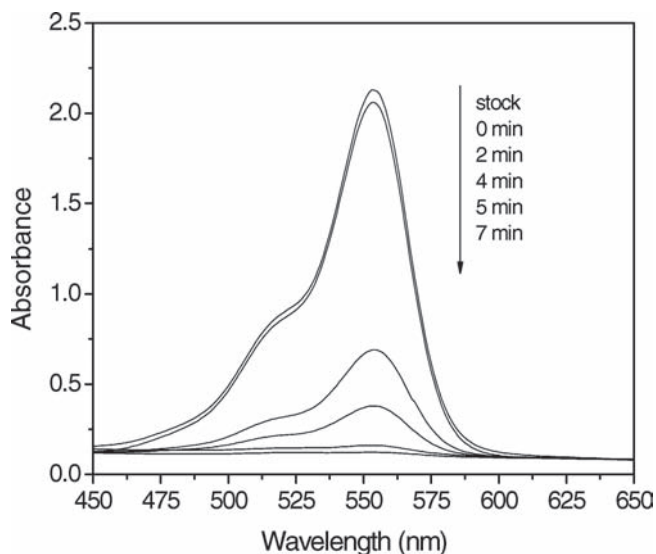


**Figure 11.** UV-vis absorption spectra of RhB during the reduction catalyzed by SPIO@NS/Au(3) composite microspheres.

progress of the reaction. It was found that the concentration of the RhB decreased a little when the SPIO@NS/Au(3) was incubated with stock solution for 30 min, which may be respond to the absorbent property of the yolk-like nanostructure (Figure S18). After the addition of NaBH<sub>4</sub>, the peak at 554 nm gradually decreases in time, indicating the reducing of the RhB dyes (Figure 11). The catalytic reduction of the dyes proceeds successfully, wherein no deactivation or poisoning of the catalyst is observed. No reaction can be observed without using the NaBH<sub>4</sub> or SPIO@NS/Au. Figure 7b shows the *M-H* curve of the as-used SPIO@NS/Au(3) composite nanocatalysts. The saturation magnetization of the product is 11 emu g<sup>-1</sup> and the value is a little smaller than the yolk-like SPIO@NS microspheres, which may be due to the loading of Au nanoparticles. The coercivity of the composite nanocatalyst approaches 0 Oe, indicating the superparamagnetic property. The as-prepared SPIO@NS/Au(3) can be efficiently recovered and recycled in the reaction mixtures by magnetic separation, which renders the catalyst cost-effective and promising for various applications.

### 3. Conclusions

We have demonstrated a facile method for the synthesis of yolk-like particles with hierarchical nickel silicate shells and movable superparamagnetic iron oxide cores. Due to the high alterability of the SPIO size, SiO<sub>2</sub> coating thickness, and the Ni<sup>2+</sup> concentration, yolk SPIO@NS microspheres with defined core size, interior cavity, and shell thickness can be technically designed. Gold nanoparticles with controllable concentration can be successfully immobilized into the above yolk-like SPIO@NS microspheres by a simple in situ reducing process and most of the Au nanoparticles are located within the hierarchical NS shells. The as-prepared SPIO@NS/Au nanocomposites show good catalytic activity using the catalytic reduction of RhB as a model reaction. These magnetically separable yolk-like SPIO@

NS particles are expected to have promising application in waste water treatment, drug delivery, and carried catalysis.

### 4. Experimental Section

**Materials:** Ferric chloride hexahydrate (FeCl<sub>3</sub>·6H<sub>2</sub>O), nickel chloride hexahydrate (NiCl<sub>2</sub>·6H<sub>2</sub>O), sodium acetate (NaOAc), sodium acrylate (Na Acrylate), ethylene glycol (EG), diethylene glycol (DEG), tetraethyl orthosilicate (TEOS), 3-aminopropyl-triethoxysilane (APTES) and urea were obtained from Aldrich. All chemicals were of analytical grade and used without further purification. Deionized water was obtained from Barnstead RO pure system and was bubbled with high-purity nitrogen for at least 30 min before use.

**Synthesis of SPIO Microspheres:** Monodispersed SPIO microspheres of various average sizes were synthesized according to our previous report.<sup>[46]</sup> Typically, for the synthesis of 200 nm SPIO microspheres, FeCl<sub>3</sub>·6H<sub>2</sub>O (2 mmol), NaOAc (1.5 g), and Na Acrylate (1.5 g) were dissolved in EG (20 mL) in a beaker. After vigorous stirring for 1 h, the homogeneous solution was transferred to a Teflon-lined stainless-steel autoclave (25 mL volume) and then sealed to heat at 200 °C. After a 12 h reaction period, the autoclave was cooled to room temperature. The obtained SPIO spheres were washed with water and ethanol, and then dispersed in water (15 mL). In this synthesis, the average sizes (20–300 nm) of the SPIO nano/micro-spheres can be controlled by varying the ratio of the solvents ( $V_{EG}/V_{DEC}$ ) in the system.

**Synthesis of SPIO@SiO<sub>2</sub> Microspheres with Core/shell Nanostructure:** The obtained SPIO microspheres were coated by a layer of SiO<sub>2</sub> shell. In particular, an aqueous solution (2.5 mL) of SPIO was diluted with water (0.5 mL) and ethanol (30 mL). The mixture was homogenized by ultrasonication for 30 min, prior to the addition of ammonia solution (1 mL). After 30 min, a solution of TEOS in ethanol was injected into the solution. The reaction was performed for 100 min and that the product was collected by the help of a magnet, and then washed with ethanol and water for several times. Finally, the product was dried in vacuum for 12 h to obtain SPIO@SiO<sub>2</sub> microspheres with core/shell nanostructure. The shell thicknesses of the SPIO@SiO<sub>2</sub> microspheres were easily controlled by varying the TEOS concentration. The size of the SPIO@SiO<sub>2</sub> microspheres can be turned by varying the SPIO core size.

**Synthesis of Yolk-like SPIO@NS Microspheres:** SPIO@SiO<sub>2</sub> core/shell particles with different sizes and shell thicknesses were dispersed in 5 mL H<sub>2</sub>O under sonication. 30 min later, 0.25 mmol NiCl<sub>2</sub>·6H<sub>2</sub>O was added into the above solution and stirred vigorously. Then, urea aqueous solution (2.25 M, 5 mL) was introduced. 20 min later, 5 mL ethanol was added under sonication. At last, the obtained solution was transferred to a Teflon-lined stainless-steel autoclave (25 mL volume) and then sealed to heat at 190 °C. After a 36 h reaction period, the autoclave was cooled to room temperature. The obtained yolk-like spheres were washed with water and ethanol, and then dried in vacuum over night.

**Synthesis of Yolk-like SPIO@NS/Au Nanocomposite:** The above SPIO@NS microspheres were firstly transferred to a mixture of isopropanol (20 mL) and APTES (0.4 mL) and heated to 80 °C for 2 h to functionalize the silicate surface with amino groups. The surface modified particles were washed with isopropanol and dispersed in deionized water. Then, the SPIO@NS/Au nanocomposites were synthesized by using an in situ reduction method. In brief, an aqueous solution (20 mL) containing yolk-like SPIO@NS microspheres and tri-sodium citrate ( $2.5 \times 10^{-4}$  M) was prepared in a conical flask. Then, HAuCl<sub>4</sub> solution was added with magnetic stirring. 1 h later, cold NaBH<sub>4</sub> solution (0.6 mL, 0.1 M) was added with vigorous stirring. The solution turned pink immediately after the addition of NaBH<sub>4</sub>, indicating Au nanoparticle formation. The SPIO@NS/Au products were magnetically separated from the solution after 1 h reaction, and rinsed by deionized water and ethanol three times. The Au weighting ratio can be controlled by varying the starting HAuCl<sub>4</sub> concentration.

**The Catalytic Reduction of RhB:** A given amount of the magnetic catalysts were added into a solution with RhB (20 mL,  $3 \times 10^{-5}$  mol L<sup>-1</sup>)

and incubated for 30 min. After that, an aqueous solution of  $\text{NaBH}_4$  (1 mL, 0.4 mol  $\text{L}^{-1}$ ) was rapidly injected at room temperature with stirring. The color of the mixture gradually vanished, indicating the reduction of the RhB dye. Changes in the concentration of RhB were monitored by examining the variations in the maximal UV/vis absorption at 554 nm. After the catalytic reaction was completed, the nanocatalysts were separated by magnetic field.

**Characterization:** X-ray powder diffraction patterns (XRD) of the products were obtained on a Bruker D8 Advance diffractometer equipped with graphite monochromatized Cu  $K\alpha$  radiation ( $\lambda = 1.5406 \text{ \AA}$ ). Transmission electron microscopy (TEM) photomicrographs were taken on a FEI CM120 microscope at an accelerating voltage of 120 kV and a high-resolution transmission electron microscope (HRTEM, Tecnai Model JEOL-2100) at an accelerating voltage of 200 kV. The magnetic properties ( $M-H$  curve) were measured at room temperature on a Lakeshore 7300 magnetometer. The field emission scanning electron microscopy (FE-SEM) images were taken on a Jeol JSM-6700F SEM. The BET tests were determined via a Micromeritics ASAP-2000 nitrogen adsorption apparatus.

## Supporting Information

Supporting Information is available from the Wiley Online Library or from the author.

## Acknowledgements

This work was supported by "the Fundamental Research Funds for the Central Universities". Supporting Information is available online from Wiley Online Library or from the author.

Received: October 18, 2010

Revised: November 30, 2010

Published online: March 28, 2011

- [1] Y. Yin, R. M. Rioux, C. K. Erdonmez, S. Hughes, G. A. Somorjai, A. P. Alivisatos, *Science* **2004**, 304, 711.
- [2] S. Kim, Y. Yin, A. P. Alivisatos, G. A. Somorjai, J. T. Yates, *J. Am. Chem. Soc.* **2007**, 129, 9510.
- [3] S. Ikeda, S. Ishino, T. Harada, N. Okamoto, T. Sakata, H. Mori, S. Kuwabata, T. Torimoto, M. Matsumura, *Angew. Chem.* **2006**, 118, 7221; *Angew. Chem., Int. Ed.* **2006**, 45, 7063.
- [4] J. Lee, J. C. Park, H. Song, *Adv. Mater.* **2008**, 20, 1523.
- [5] X. Q. Huang, C. Y. Guo, L. Q. Zuo, N. F. Zheng, G. D. Stucky, *Small* **2009**, 5, 361.
- [6] X. W. Lou, L. A. Archer, Z. C. Yang, *Adv. Mater.* **2008**, 20, 3987.
- [7] Y. Zhao, L. Jiang, *Adv. Mater.* **2009**, 21, 3621.
- [8] K. Kamata, Y. Lu, Y. N. Xia, *J. Am. Chem. Soc.* **2003**, 125, 2384.
- [9] Q. Zhang, T. R. Zhang, J. P. Ge, Y. D. Yin, *Nano Lett.* **2008**, 8, 2867.
- [10] M. Kim, K. Sohn, Bin H. Na, T. Hyeon, *Nano Lett.* **2002**, 2, 1383.
- [11] K. Zhang, X. Zhang, H. Chen, X. Chen, L. Zheng, J. Zhang, B. Yang, *Langmuir* **2003**, 20, 11312.
- [12] D. M. Cheng, X. D. Zhou, H. B. Xia, H. S. O. Chan, *Chem. Mater.* **2005**, 17, 3578.
- [13] X. J. Wu, D. S. Xu, *J. Am. Chem. Soc.*, **2009**, 131, 2774.
- [14] F. Caruso, R. A. Caruso, H. Mohwald, *Science* **1998**, 282, 1111.
- [15] S. M. Marinakos, J. P. Novak, L. C. Brousseau, A. B. House, E. M. Edeki, J. C. Feldhaus, D. L. Feldheim, *J. Am. Chem. Soc.* **1999**, 121, 8518.
- [16] X. W. Lou, C. Yuan, E. Rhoades, Q. Zhang, L. A. Archer, *Adv. Funct. Mater.* **2006**, 16, 1679.
- [17] P. Jiang, J. F. Bertone, V. L. Colvin, *Science* **2001**, 291, 453.
- [18] W. Zhao, H. Chen, Y. Li, L. Li, M. Lang, J. Shi, *Adv. Funct. Mater.* **2008**, 18, 2780.
- [19] Y. Zhu, E. Kockrick, T. Ikoma, N. Hanagata, S. Kaskel, *Chem. Mater.* **2009**, 21, 2547.
- [20] L. Y. Hao, S. H. Xuan, X. L. Gong, R. Gu, W. Q. Jiang, Z. Y. Chen, *Chem. Lett.* **2007**, 1, 126.
- [21] S. Xuan, F. Liang, K. Shu, *J. Magn. Magn. Mater.* **2009**, 321, 1029.
- [22] X. W. Lou, C. Yuan, L. A. Archer, *Adv. Mater.* **2007**, 19, 3328.
- [23] X. W. Lou, L. A. Archer, *Adv. Mater.* **2008**, 20, 1853.
- [24] U. Jeong, X. Teng, Y. Wang, H. Yang, Y. Xia, *Adv. Mater.* **2007**, 19, 33.
- [25] F. Bai, D. S. Wang, Z. Y. Huo, W. Chen, L. P. Liu, X. Liang, C. Chen, X. Wang, Q. Peng, Y. D. Li, *Angew. Chem., Int. Ed.* **2007**, 46, 6650.
- [26] J. Q. Zhuang, H. M. Wu, Y. G. Yang, Y. C. Cao, *J. Am. Chem. Soc.* **2007**, 129, 14166.
- [27] J. Ge, Y. Hu, M. Biasini, W. P. Beyermann, Y. Yin, *Angew. Chem., Int. Ed.* **2007**, 46, 4342.
- [28] A. H. Lu, E. L. Salabas, F. Schuth, *Angew. Chem., Int. Ed.* **2007**, 46, 1222.
- [29] S. Sun, H. Zeng, *J. Am. Chem. Soc.* **2002**, 124, 8204.
- [30] H. Deng, X. Li, Q. Peng, X. Wang, J. Chen, Y. Li, *Angew. Chem., Int. Ed.* **2005**, 44, 2782.
- [31] S. H. Xuan, F. Wang, Y. X. J. Wang, J. C. Yu, K. C. F. Leung, *J. Mater. Chem.* **2010**, 20, 5086.
- [32] Y. Chen, H. R. Chen, L. M. Guo, Q. J. He, F. Chen, J. Zhou, J. W. Feng, J. L. Shi, *ACS Nano* **2010**, 4, 529.
- [33] Y. Q. Wang, G. Z. Wang, H. Q. Wang, C. H. Liang, W. P. Cai, L. D. Zhang, *Chem. Eur. J.* **2010**, 16, 3497.
- [34] L. S. Zhong, J. S. Hu, H. P. Liang, A. M. Cao, W. G. Song, L. J. Wan, *Adv. Mater.* **2006**, 18, 2426.
- [35] J. Zheng, B. H. Wu, Z. Y. Jiang, Q. Kuang, X. L. Fang, Z. X. Xie, R. B. Huang, L. S. Zheng, *Chem. Asia. J.* **2010**, 16, 3497.
- [36] M. Dogan, Y. Ozdemir, M. Alkan, *Dyes Pigm.* **2007**, 75, 701.
- [37] N. Bektas, B. A. Agim, S. Kara, *J. Hazard. Mater.* **2004**, 112, 115.
- [38] H. J. Hah, J. I. Um, S. H. Han, S. M. Koo, *Chem. Commun.* **2004**, 8, 1012.
- [39] D. K. Yi, S. S. Lee, J. Y. Ying, *Chem. Mater.* **2006**, 18, 2459.
- [40] S. Shylesh, V. Schunemann, W. R. Thiel, *Angew. Chem., Int. Ed.* **2010**, 49, 3428.
- [41] J. P. Ge, Q. Zhang, T. R. Zhang, Y. D. Yin, *Angew. Chem., Int. Ed.* **2008**, 47, 8924.
- [42] M. Feyen, C. Weidenthaler, F. Scheuth, A. H. Lu, *Chem. Mater.* **2010**, 22, 2955.
- [43] Y. H. Deng, Y. Cai, Z. K. Sun, J. Liu, C. Liu, J. Wei, W. Li, C. Liu, Y. Wang, D. Y. Zhao, *J. Am. Chem. Soc.* **2010**, 132, 8466.
- [44] P. Jin, Q. W. Chen, L. Q. Hao, R. F. Tian, L. X. Zhang, L. Wang, *J. Phys. Chem. B* **2004**, 108, 6311.
- [45] D. B. Wang, C. X. Song, Z. S. Hu, X. Fu, *J. Phys. Chem. B* **2005**, 109, 1125.
- [46] S. H. Xuan, Y. X. J. Wang, J. C. Yu, K. C. F. Leung, *Chem. Mater.* **2009**, 21, 5079.
- [47] J. P. Ge, Y. D. Yin, *Adv. Mater.* **2008**, 20, 3485.
- [48] Y. Q. Wang, G. Z. Wang, H. Q. Wang, W. P. Cai, C. H. Liang, L. D. Zhang, *Nanotechnology* **2009**, 20, 155604.
- [49] J. Wang, Y. J. Zhu, Y. J. Wu, C. J. Wu, D. F. Xu, Z. Zhang, *Mod. Phys. Lett. B* **2006**, 10, 549.
- [50] S. H. Xuan, Y. X. J. Wang, J. C. Yu, K. C. F. Leung, *Langmuir* **2009**, 25, 11835.
- [51] Q. Zhang, J. P. Ge, J. Goebel, Y. X. Hu, Y. G. Sun, *Adv. Mater.* **2010**, 22, 1905.
- [52] H. J. Chen, L. Shao, K. C. Woo, T. Ming, H. Q. Lin, J. F. Wang, *J. Phys. Chem. C* **2009**, 113, 17691.
- [53] T. Ming, L. Zhao, Z. Yang, H. J. Chen, L. D. Sun, J. F. Wang, C. H. Yan, *Nano Lett.* **2009**, 9, 3896.
- [54] S. Z. Zhang, W. H. Ni, X. S. Kou, M. H. Yeung, L. D. Sun, J. F. Wang, C. H. Yan, *Adv. Funct. Mater.* **2007**, 17, 3258.